J. Math. Biol. (2017) 74:1627–1656
DOI 10.1007/s00285-016-1066-5

Mathematical Biology

Robust phase-waves in chains of half-center oscillators

Calvin Zhang[1] · **Timothy J. Lewis**[2]

Received: 28 October 2015 / Revised: 16 June 2016 / Published online: 13 October 2016

Abstract Many neuronal circuits driving coordinated locomotion are composed of chains of half-center oscillators (HCOs) of various lengths. The HCO is a common motif in central pattern generating circuits (CPGs); an HCO consists of two neurons, or two neuronal populations, connected by reciprocal inhibition. To maintain appropriate motor coordination for effective locomotion over a broad range of frequencies, chains of CPGs must produce approximately constant phase-differences in a robust manner. In this article, we study phase-locking in chains of nearest-neighbor coupled HCOs and examine how the circuit architecture can promote phase-constancy, i.e., inter-HCO phase-differences that are frequency-invariant. We use two models with different levels of abstraction: (1) a conductance-based model in which each neuron is modeled by the Morris–Lecar equations (the ML-HCO model); and (2) a coupled phase model in which the state of each HCO is captured by its phase (the phase-HCO model). We show that one of four phase-waves with inter-HCO phase-differences at approximately 0, 25, 50 or 75 % arises robustly as a result of the inter-HCO connection topology, and its robust existence is not affected by the number of HCOs in the chain, the difference in strength between the ascending and descending nearest-neighbor connections, or the number of nearest-neighbor connections. Our results show that the internal anti-phase structure of the HCO and an appropriate inter-HCO connection topology together can provide a mechanism for robust (i.e., frequency-independent) limb coordination in

✉ Calvin Zhang
calvinz@cims.nyu.edu

Timothy J. Lewis
tjlewis@ucdavis.edu

[1] Courant Institute of Mathematical Sciences, 251 Mercer Street, New York, NY 10012, USA

[2] Department of Mathematics, University of California, Davis, One Shields Ave, Davis, CA 95616, USA

segmented animals, such as the 50 % interlimb phase-differences in the tripod gate of stick insects and cockroaches, and the 25 % interlimb phase-differences in crayfish and other long-tailed crustaceans during forward swimming.

Keywords Phase constancy · Phase-wave · Central pattern generator · Half-center oscillator · Metachronal coordination

Mathematics Subject Classification 34C15 · 92C20

1 Introduction

A fundamental challenge in neuroscience is to understand how nervous systems produce coordinated rhythmic motor behaviors, such as walking, swimming, breathing, and chewing. Often these coordinated rhythms must be *robust* in the sense that they need to be maintained over a significant variation in frequency. For example, when we walk, the left leg and the right leg move in anti-phase (i.e., the limbs are phase-locked with a phase-difference of 50 % of the period), regardless of the walking frequency. This frequency-invariant phase-locking is known as *phase constancy* and is commonly seen in animal locomotion (Hill et al. 2003). Other examples of phase constancy include: (1) the symmetric tripod walking gait in cockroaches and stick insects, in which neighboring limbs are always in anti-phase (Daun-Gruhn and Toth 2011; Proctor et al. 2010); (2) forward swimming of long-tailed crustaceans such as lobsters, shrimp, or crayfish, in which four or five pairs of limbs move rhythmically in a back-to-front metachronal wave with 25 % phase-differences between neighboring limbs (Mulloney and Smarandache-Wellmann 2012), and (3) the undulatory locomotion in lamprey and leech swimming, in which the approximate 100 and 32 body segments produce a wave-like flexural movement with an approximate 1 and 3 % phase-lag between neighboring segments such that the undulations of a single body length are maintained (Sigvardt and Miller 1974; Kristan et al. 1974).

Almost all rhythmic movements in animals are driven, at least in part, by networks of interconnected central pattern generators (CPGs). CPGs are specialized neuronal circuits in the central nervous system that produce endogenously rhythmic activities without requiring afferent feedback or rhythmic input (Hooper 2001). The kernel of many CPGs, especially those associated with locomotor rhythms, are half-center oscillators (HCOs) (Mulloney and Smarandache 2010; Ijspeert 2008; Grillner 2006; Hooper 2001). An HCO consists of two neurons, or two neuronal populations, connected by reciprocal inhibition. The mutual inhibition, along with some form of slow adaptation, produces anti-phase oscillations between the two internal units in which each unit alternates between an active state and a suppressed state (Skinner et al. 1994; Wang and Rinzel 1992). Many neuronal circuits driving body or limb movements in segmented animals are composed of a chain of HCOs of different lengths (Mulloney and Smarandache 2010; Ijspeert 2008; Stein 2007; Grillner 2006; Marder and Calabrese 1996; Cohen and Kiemel 1993). A chain with four or five pairs of HCOs produces the metachronal swimmeret coordination in long-tailed crustaceans (Mulloney and Smarandache-Wellmann 2012), a chain of 3 HCOs helps produce different

gaits in the legged locomotion of insects (Daun-Gruhn and Toth 2011; Proctor et al. 2010), and a chain of approximately 100 HCOs drives the undulatory body movement of lamprey (Cohen et al. 1992). All of these systems display *phase-waves* in chains of HCOs that are robust to variations in frequency. (Here, we define phase-waves to be phase-locked states with approximately constant phase-differences between neighboring segments). Therefore, an understanding of the neural underpinning of robust locomotion relies on an understanding of phase-waves in chains of HCOs of different lengths.

This article presents a general mathematical treatment of phase-waves in chains of nearest-neighbor coupled HCOs with an arbitrary length. The motivation for this work stems primarily from the study of the forward-swimming in crustaceans (Zhang et al. 2014; Mulloney and Smarandache-Wellmann 2012). As mentioned above, crayfish, krill, and other long-tailed crustaceans swim forward by rhythmically paddling pairs of abdominal limbs, known as swimmerets, in a back-to-front phase-wave with 25 % inter-segmental phase-differences despite large variations in the stroke frequency. Smarandache et al. (2009) showed that, in crayfish, this back-to-front phase-wave is centrally generated by a chain of four HCOs with a particular asymmetric inter-HCO connection topology. Recently, we demonstrated that the half-center structure of the HCO and the experimentally-identified asymmetric inter-HCO connection topology Zhang et al. (2014) combine to provide a robust mechanism for generating this 25 % phase-constant rhythm. This previous result is for the crayfish swimmeret neural circuit that is composed of a chain of four HCOs. As mentioned above, locomotor behaviors of many other animals are driven by chains of HCOs of different lengths. In this article, we extend the analysis in Zhang et al. (2014) to chains of HCOs with an arbitrary length. We also relax several crucial assumptions made in Zhang et al. (2014) about the inter-HCO connections. Specifically, we study the existence and stability of four robust phase-waves (in-phase, 25 % phase-locking, anti-phase and 75 % phase-locking), or small deviations from these exact phase-waves, in chains of n HCOs with nearest-neighbor inter-HCO connections for any integer $n \geq 2$. We note that a large body of previous work has addressed the existence and stability of phase-locked states in chains of oscillators (e.g., Várkonyi et al. (2008), Skinner and Mulloney (1998), Ren and Ermentrout (1998), Kopell and Ermentrout (1986)). Here, we focus on how the *internal structure* of the HCOs combines with the *inter-HCO connectivity* to influence the conditions for the robust existence and stability of phase-waves and thus the conditions for these states to display phase constancy.

The outline for the remainder of this paper is as follows. In Sect. 2, we construct a conductance-based model of a chain of HCOs (the ML-HCO model) and examine the effects of the network topology of the nearest-neighbor inter-HCO connections on phase-locking. In the ML-HCO model, each internal neuron in an HCO is modeled by the Morris-Lecar equations so that we can examine the robustness of phase-locking against variations in the intrinsic frequency of each HCO. We observe that one of four phase-waves [in-phase (0 %), 25 %, anti-phase (50 %), or 75 %] arises in chains of HCOs with various lengths, largely *independent* of the frequency of oscillation, as long as the internal units in each HCO remain close to their normal anti-phase state. In Sect. 3, we develop a coupled phase model (the phase-HCO

model) for a chain of HCOs in which the state of each HCO is given by a single variable, its phase. This phase reduction allows us to derive closed-form expressions of the existence and the stability conditions of the four different robust phase-waves and to demonstrate how the robustness of the phase-waves is a consequence of the half-center structure of the HCO and of the inter-HCO connection topology. In Sect. 4, we consider the effects of variations in the number and strength of the ascending and descending inter-HCO connections. Finally, in Sect. 5, we analyze robust phase-locking in rings of HCOs with different numbers of HCOs and contrast it to that in the chains. Our results imply that the mutual inhibition within the HCO together with an appropriate inter-segmental connection topology in chains of HCOs promote phase constancy and are thus functionally significant for animal locomotion.

2 Robust phase-waves in chains of HCOs: results of a conductance-based model

In this section, we consider a conductance-based cellular model for chains of nearest-neighbor coupled HCOs of various lengths. We proceed as follows: (1) We first construct a model for each local HCO, and then (2) we describe the fundamentally different inter-HCO connection topologies and couple the HCOs to obtain a full model of the neural circuit. Using this model, we perform a series of numerical experiments to show that different inter-HCO connection topologies lead to different robust phase-waves.

2.1 A conductance-based model of chains of HCOs

2.1.1 Dynamics of the isolated HCOs

Recall that HCOs are composed of two neurons (or two neuronal populations) coupled by strong mutual inhibition. Various models have been proposed to describe the dynamics of HCOs (e.g., Clewley (2011), Taylor et al. (2002), Skinner et al. (1994), Wang and Rinzel (1992)). Here, we use the HCO model described by Skinner et al. (1994): The intrinsic dynamics of each neuron in the HCO is modeled by the Morris–Lecar equations, which include an instantaneous voltage-dependent inward Ca^{2+} current, an outward K^+ current, and a linear leakage current. The state of each neuron in the HCO model is described by two dynamic variables: the membrane potential V_i, and the gating variable N_i for the K^+ current, in which i is the index of the internal neuron ($i = 1, 2$). The synaptic conductance of the reciprocal inhibition is modeled by an instantaneous function of the presynaptic membrane potential. Note that the model does not include ionic currents that underlie fast spikes. Therefore, the voltage of the model during the active state should be interpreted as the actual membrane potential of a non-spiking cell, or it can be interpreted as the voltage envelope during a burst of action potentials in a spiking neuron.

The HCO model equations are

$$\begin{cases} C\dfrac{dV_i}{dt} = -g_{\mathrm{Ca}} m_\infty(V_i)\Big(V_i - E_{\mathrm{Ca}}\Big) - g_{\mathrm{K}} N_i\Big(V_i - E_{\mathrm{K}}\Big) - g_L\Big(V_i - E_L\Big) \\ \qquad\qquad + I_{\mathrm{bias}} - g_{\mathrm{syn}}^{\mathrm{local}} s_{j\to i}(V_j)\Big(V_i - E_{\mathrm{syn}}^{\mathrm{local}}\Big), \\ \dfrac{dN_i}{dt} = \dfrac{\phi_N}{\tau_N(V_i)}\Big(N_\infty(V_i) - N_i\Big), \quad (i, j = 1, 2;\ i \neq j) \end{cases} \tag{1}$$

in which g_{Ca} is the maximum conductance of the Ca^{2+} current, g_{K} is the maximum conductance of the K^+ current, g_L is the conductance of the leakage current, and the product $g_{\mathrm{syn}}^{\mathrm{local}} s_{j\to i}$ is the postsynaptic conductance in neuron i due to activity in neuron j; $\eta_{\mathrm{syn}}^{\mathrm{local}}$ and k_{syn} are the synaptic threshold and gain, respectively; E_{Ca}, E_{K}, E_{L}, and $E_{\mathrm{syn}}^{\mathrm{local}}$ are the reversal potentials of the Ca^{2+}, K^+, leakage, and synaptic currents, respectively; I_{bias} is the bias current, and C is the membrane capacitance. The voltage dependent gating functions are

$$m_\infty(V_i) = \frac{1}{2}\left(1 + \tanh\left(\frac{V_i}{15}\right)\right), \tag{2}$$

$$N_\infty(V_i) = \frac{1}{2}\left(1 + \tanh\left(\frac{V_i}{15}\right)\right). \tag{3}$$

We assume that $s_{j\to i}$ is a sigmoidal function of the presynaptic voltage defined by

$$s_{j\to i}\left(V_j\right) = \frac{1}{2}\left(1 + \tanh\left(\frac{V_j - \eta_{\mathrm{syn}}^{\mathrm{local}}}{k_{\mathrm{syn}}^{\mathrm{local}}}\right)\right). \tag{4}$$

The rate at which the K^+ conductance activates and deactivates is $\phi_N/\tau_N(V_i)$, in which $\phi_N = 0.005$ and

$$\tau_N(V_i) = \cosh^{-1}\left(\frac{V_i}{30}\right). \tag{5}$$

Periodic anti-phase oscillations between the two internal units are obtained with $g_{\mathrm{Ca}} = 0.015$ mS/cm^2, $g_{\mathrm{K}} = 0.02$ mS/cm^2, $g_{\mathrm{syn}}^{\mathrm{local}} = 0.01$mS/cm^2, $\eta_{\mathrm{syn}}^{\mathrm{local}} = 20$ mV, $k_{\mathrm{syn}} = 2$, $I_{\mathrm{bias}} = 0.8$ mA/cm^2, $E_{\mathrm{Ca}} = 100$ mV, $E_{\mathrm{K}} = -80$ mV, $E_{\mathrm{L}} = -30$ mV, $E_{\mathrm{syn}}^{\mathrm{local}} = -80$mV, and $C = 1\mu$F/cm^2. Modulation of the frequency of the oscillations is achieved by adjusting the conductance of the leakage current g_L of both internal neurons. Figure 1 illustrates that as we increase g_L from 0.003 to 0.011 mS/cm^2, the frequency of an isolated HCO increases from about 1.4–2.4 Hz. Beyond these values of g_L, oscillations are lost via a Hopf bifurcation.

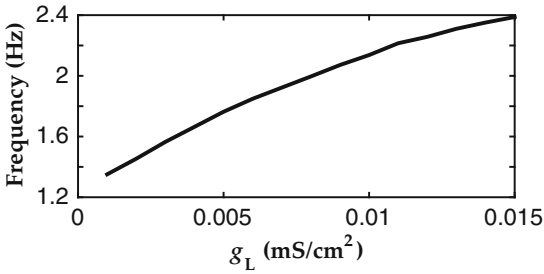

Fig. 1 The frequency of oscillation in an isolated HCO as a function of the conductance of the leakage current g_L. Other parameters are defined in the main text

To rewrite the HCO model equations (Eq. 1) in a compact manner, we define

$$\begin{aligned} f(V_i, V_j, N_i) &= \frac{1}{C}\Big(- g_{\mathrm{Ca}} m_\infty(V_i)\Big(V_i - E_{\mathrm{Ca}}\Big) - g_{\mathrm{K}} N_i \Big(V_i - E_{\mathrm{K}}\Big) \\ &\quad - g_L\Big(V_i - E_L\Big) + I_{\mathrm{bias}} - g_{\mathrm{syn}}^{\mathrm{local}} s_{j\to i}(V_j)\Big(V_i - E_{\mathrm{syn}}^{\mathrm{local}}\Big)\Big), \\ g(V_i, N_i) &= \frac{\phi_N}{\tau_N(V_i)}\Big(N_\infty(V_i) - N_i\Big), \end{aligned} \tag{6}$$

and

$$\mathbf{F}(\mathbf{X}) = \begin{pmatrix} f(V_1, V_2, N_1) \\ f(V_2, V_1, N_2) \\ g(V_1, N_1) \\ g(V_2, N_2) \end{pmatrix}, \tag{7}$$

where $\mathbf{X} = (V_1, V_2, N_1, N_2)$. Thus the HCO model equations (Eq. 1) can be rewritten as

$$\frac{d\mathbf{X}}{dt} = \mathbf{F}(\mathbf{X}). \tag{8}$$

2.1.2 Inter-HCO connections: dynamics and topology

Having defined the model of each local HCO unit, we now describe the synaptic connections between the HCOs. We assume that each HCO is coupled with its nearest neighbor(s) only. We initially assume that all ascending and descending connections have the same dynamics and strength, and that there are at most one ascending and one descending connection incident on each HCO. These assumptions, however, will be removed in Sect. 4 to allow variations in the strength and the number of inter-HCO connections. The case of a single ascending and a single descending input to HCOs applies directly to the neural circuit underlying the crayfish swimmeret system (Mulloney and Smarandache-Wellmann 2012), in which the four swimmerets on each side of the body are driven by a chain of HCOs. However, the removal of these constraints on the connection topology in Sect. 4 allows us to generalize our results to neural circuits in which HCOs receive multiple ascending and descending inputs,

e.g., the locomotor circuits of the stick insect (Toth et al. 2015; Daun-Gruhn and Toth 2011), lamprey (Grillner 2006; Ijspeert and Kodjabachian 1999; Cohen et al. 1982) and salamander (Chevalliera et al. 2008; Ijspeert 2008; Ijspeert et al. 2007).

Let $V_i^{(k)}$ be the membrane potential of neuron i in the k-th HCO, in which $i = 1, 2$ and $k = 1, 2, \ldots, n$. Similar to the synaptic coupling between the two internal neurons in each HCO, the inter-HCO synaptic connection from neuron j in the l-th HCO to neuron i in the k-th HCO is described using an instantaneous synaptic current defined by

$$I_{\text{syn}}^{\text{inter}}\left(V_i^{(k)}, V_j^{(l)}\right) = g_{\text{syn}}^{\text{inter}} S_{\infty}^{\text{inter}}\left(V_j^{(l)}\right)\left(V_i^{(k)} - E_{\text{syn}}^{\text{inter}}\right), \tag{9}$$

where

$$S_{\infty}^{\text{inter}}(V_j^{(l)}) = \left(1 + e^{-(V_j^{(l)} - \eta_{\text{syn}}^{\text{inter}})/k_{\text{syn}}^{\text{inter}}}\right)^{-1}, \tag{10}$$

in which the maximum conductance of the inter-HCO synaptic connections is $g_{\text{syn}}^{\text{inter}} = 0.001\ \text{mS/cm}^2$, the reversal potential of the inter-HCO synaptic connections is $E_{\text{syn}}^{\text{inter}} = 80$ mV, and the parameters associated with the activation and deactivation of the synaptic connections are $k_{\text{syn}}^{\text{inter}} = 2$, $\eta_{\text{syn}}^{\text{inter}} = -20$ mV.

Thus, the complete conductance-based model of a chain of n HCOs with nearest-neighbor coupling is

$$\begin{cases} \dfrac{d\mathbf{X}^{(1)}}{dt} = \mathbf{F}(\mathbf{X}^{(1)}) - \dfrac{1}{C} I_{\text{syn}}^{\text{inter}}\left(V_j^{(1)}, V_i^{(2)}\right)\mathbf{e}_j, \\ \dfrac{d\mathbf{X}^{(k)}}{dt} = \mathbf{F}(\mathbf{X}^{(k)}) - \dfrac{1}{C}\left(I_{\text{syn}}^{\text{inter}}\left(V_j^{(k)}, V_i^{(k+1)}\right)\mathbf{e}_j + I_{\text{syn}}^{\text{inter}}\left(V_j^{(k)}, V_i^{(k-1)}\right)\mathbf{e}_j\right), \\ \quad \text{for } \ k = 2, 3, \ldots, n-1, \\ \dfrac{d\mathbf{X}^{(n)}}{dt} = \mathbf{F}(\mathbf{X}^{(n)}) - \dfrac{1}{C} I_{\text{syn}}^{\text{inter}}\left(V_j^{(n)}, V_i^{(n-1)}\right)\mathbf{e}_j, \end{cases} \tag{11}$$

in which $\mathbf{e}_1 = (1, 0, 0, 0)$, $\mathbf{e}_2 = (0, 1, 0, 0)$, and $\mathbf{X}^{(k)} = \left(V_1^{(k)}, V_2^{(k)}, N_1^{(k)}, N_2^{(k)}\right)$. In Eq. 11, the indices i and j are not constant but rather placeholders that take the value of 1 or 2. j is the index that corresponds to the internal neuron in the presynaptic HCO, and i is the index that corresponds to the internal neuron in the postsynaptic HCO. However, the j in $\mathbf{e}_j$ always matches the j in the preceding function $I_{\text{syn}}^{\text{inter}}$.

If there is only one ascending and one descending connection between neighboring HCOs, then there are 16 possible topologies if we do not immediately distinguish the difference between inhibitory and excitatory connections. Using the symmetry that the two internal neurons in each HCO are identical and are always in anti-phase, the 16 possible topologies are reduced to four *fundamentally* different inter-HCO connection topologies: (s1), (s2), (a1), and (a2). See Table 1 and Fig. 3.

Table 1 The four fundamentally different inter-HCO connection topologies

Inter-HCO connection	Topology (s1)	Topology (s2)	Topology (a1)	Topology (a2)
$(k+1)$-th HCO to k-th HCO (ascending)	$I_{\text{syn}}^{\text{inter}}(V_1^{(k)}, V_1^{(k+1)})(\phi_{\text{A}} = 0)$	$I_{\text{syn}}^{\text{inter}}(V_1^{(k)}, V_2^{(k+1)})(\phi_{\text{A}} = 0.5)$	$I_{\text{syn}}^{\text{inter}}(V_2^{(k)}, V_2^{(k+1)})(\phi_{\text{A}} = 0)$	$I_{\text{syn}}^{\text{inter}}(V_1^{(k)}, V_2^{(k+1)})(\phi_{\text{A}} = 0.5)$
k-th HCO to $(k+1)$-th HCO (descending)	$I_{\text{syn}}^{\text{inter}}(V_1^{(k+1)}, V_1^{(k)})(\phi_{\text{D}} = 0)$	$I_{\text{syn}}^{\text{inter}}(V_1^{(k+1)}, V_2^{(k)})(\phi_{\text{D}} = 0.5)$	$I_{\text{syn}}^{\text{inter}}(V_2^{(k+1)}, V_1^{(k)})(\phi_{\text{D}} = 0.5)$	$I_{\text{syn}}^{\text{inter}}(V_1^{(k+1)}, V_1^{(k)})(\phi_{\text{D}} = 0)$

See Fig. 3 for illustrations

1. In inter-HCO connection topology (s1), the ascending connection from HCO-$(k+1)$ to HCO-k is from Neuron 1 to Neuron 1, and the descending connection from HCO-k to HCO-$(k+1)$ is also from Neuron 1 to Neuron 1.
2. In inter-HCO connection topology (s2), the ascending connection from HCO-$(k+1)$ to HCO-k is from Neuron 2 to Neuron 1, and the descending connection from HCO-k to HCO-$(k+1)$ is also from Neuron 2 to Neuron 1.
3. In inter-HCO connection topology (a1), the ascending connection from HCO-$(k+1)$ to HCO-k is from Neuron 2 to Neuron 2, but the descending connection from HCO-k to HCO-$(k+1)$ is from Neuron 2 to Neuron 1.
4. In inter-HCO connection topology (a2), the ascending connection from HCO-$(k+1)$ to HCO-k is from Neuron 1 to Neuron 2, but the descending connection from HCO-k to HCO-$(k+1)$ is from Neuron 1 to Neuron 1.

Inter-HCO connection topologies (s1) and (s2) are symmetric in the sense that both the ascending and descending connections go from the same internal neuron to another same internal neuron, whereas the inter-HCO connection topologies (a1) and (a2) are asymmetric because one of the two connections goes from Neuron 1 to Neuron 1 (or from Neuron 2 to Neuron 2) but the other connection goes from Neuron 1 to Neuron 2 (or from Neuron 2 to Neuron 1).

2.2 The four robust phase-waves in chains of HCOs with different lengths

Here, we examine the phase-locking dynamics of the conductance-based model of the HCO chain (Eq. 11) under different excitatory inter-HCO connection topologies, different lengths, and different frequencies of oscillations.

Figure 2 provides an example of the phase-locking dynamics in a chain of four HCOs with excitatory inter-HCO connections under the (a1) network topology, where $\Delta\theta_1 = 0.29$, $\Delta\theta_2 = 0.27$, $\Delta\theta_3 = 0.24$. That is, the phase-differences between the three neighboring pairs of HCOs are approximately 25 % of the period, forming a "25 % phase-wave" (i.e., $\Delta\theta_k = \Delta\theta^* \approx 0.25$ for all k). Moreover, we see that $\Delta\theta_1 > \Delta\theta_2 > \Delta\theta_3$. (These small systematic deviations in phase-lag along the HCO chain are explained in Sect. 3.2.3.) Experimental observations in the crayfish swimmeret system is consistent with this model prediction (Smarandache et al. 2009).

In general, we find that phase-waves with four different inter-HCO phase-differences emerge under different inter-HCO connection topologies. Topology (s1) produces an approximate in-phase activity (i.e., 0 % phase-wave), topology (s2) produces an approximate anti-phase (50 %) phase-wave, topology (a1) produces an approximate 25 % phase-wave, and topology (a2) produces an approximate 75% phase-wave. These phase-waves are robust against changes in the frequency of oscillation, i.e., they are *phase-constant* rhythms. Furthermore, they are largely independent of the length of the chain.

The panels in the top row of Fig. 4 show the phase-difference between a pair of coupled HCOs (i.e., a "chain" of two HCOs) as a function of the frequency of oscillation under the four fundamentally different inter-HCO connection topologies. Stable in-phase and anti-phase phase-locking exist under the symmetric topologies

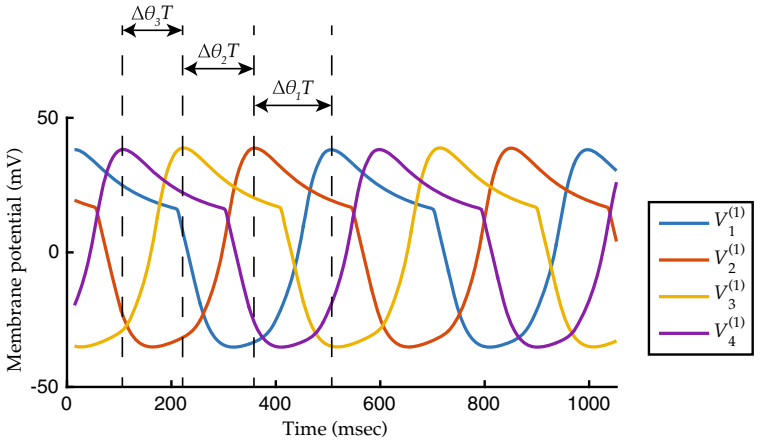

Fig. 2 Membrane potentials of the internal Neuron 1's in a chain of four HCOs under the asymmetric inter-HCO connection topology (a1). The inter-HCO connection topology is defined in Table 1. Membrane potentials $V_k^{(1)}$ of the four internal Neuron 1's in the corresponding four HCOs are plotted in separate curves indicated in the legend. Phase-differences between each neighboring HCOs, $\Delta\theta_k = \theta_{k+1} - \theta_k$, are indicated in the figure. The phase-difference θ_k between HCO-$(k+1)$ and HCO-k is given by the time lag between the membrane potential peaks of the two adjacent HCOs normalized by the period of oscillation T of the HCOs (color figure online)

(s1) and (s2), respectively; whereas stable phase-locking with 25 and 75 % phase-differences exist under the asymmetric topologies (a1) and (a2), respectively. These phase-differences remain approximately constant over a two-fold change in frequency, which is the entire frequency range of the HCOs. Note that, in almost all cases of chains with three or more HCOs, there is a systematic variation in phase-differences along the chain, $\Delta\theta_k > \Delta\theta_{k+1}$. In Sect. 3.2.3, we show that these systematic deviations in phase-lag along the chain result from "end effects", in the sense that the HCOs on the two ends of the chain receive a different number of inter-HCO connections than the HCOs in the middle of the chain.

Despite an increase in the number of HCOs in the chains, the four robust phase-waves persist. The panels in the middle and bottom rows of Fig. 4 show the phase-differences between neighboring HCO pairs in a chain of four HCOs and in a chain of 9 HCOs, respectively. While these longer chains of HCOs do not display perfect phase-waves, they exhibit approximate phase-waves. That is, there are only small variations in the inter-HCO phase-differences along the chain, and these phase-differences exhibit very little frequency dependence. Under topology (s1), inter-HCO phase-differences are around 0 (approximately in-phase), and under topology (s2), the phase-differences are around 50 % (approximately anti-phase). Chains with topology (a1) and topology (a2) display approximate 25 % phase-wave and 75 % phase-wave, respectively. Note that the chain of four HCOs with inter-HCO connection topology (a1) corresponds to the topology in the natural neuronal circuit underlying the crayfish swimmeret system, and this numerical experiment produces the desired 25 % back-to-front phase-wave

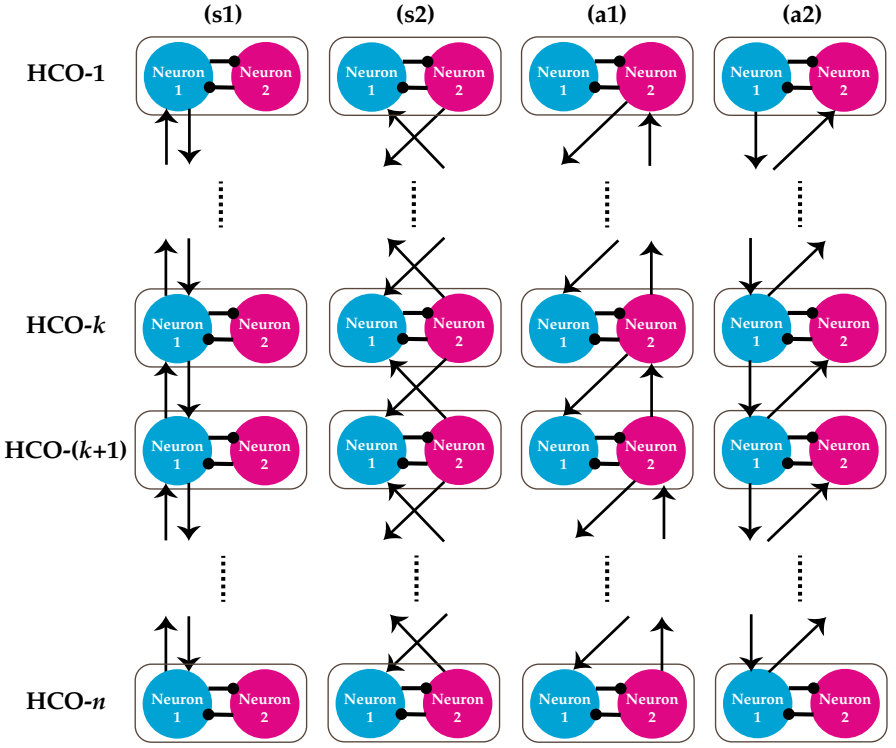

Fig. 3 The four fundamentally different inter-HCO connection topologies. The network topologies are defined in Table 1. Each HCO consists of two internal neurons, labeled as Neuron 1 (*blue*) and Neuron 2 (*pink*). These two internal neurons are mutually coupled via strong inhibitory synapses, illustrated by line segments with a *solid circle* on the target end. The inter-HCO synaptic connections are plotted as *line segments* with an *arrow* on the target end; they can be either effectively excitatory or inhibitory (color figure online)

observed in the coordinated movement of the swimmerets during crayfish's forward swimming (Mulloney and Smarandache-Wellmann 2012).

3 Robust phase-waves in chains of HCOs: an analysis of a coupled phase model

The above numerical experiments of the conductance-based model of chains of HCOs have shown that four particular phase-waves can exist in chains of HCOs with various lengths over a wide variety of conditions including the variation of frequency. In this section, we describe the mechanisms through which the inter-HCO connection topology promotes the robust existence of these phase-waves. To do so, we employ a coupled phase model that captures the essential properties of the internal HCO structure and the inter-HCO connectivity. Note that the conductance-based model can be systematically reduced to the coupled phase model in the limit of weak inter-HCO connectivity (Schwemmer and Lewis 2012).

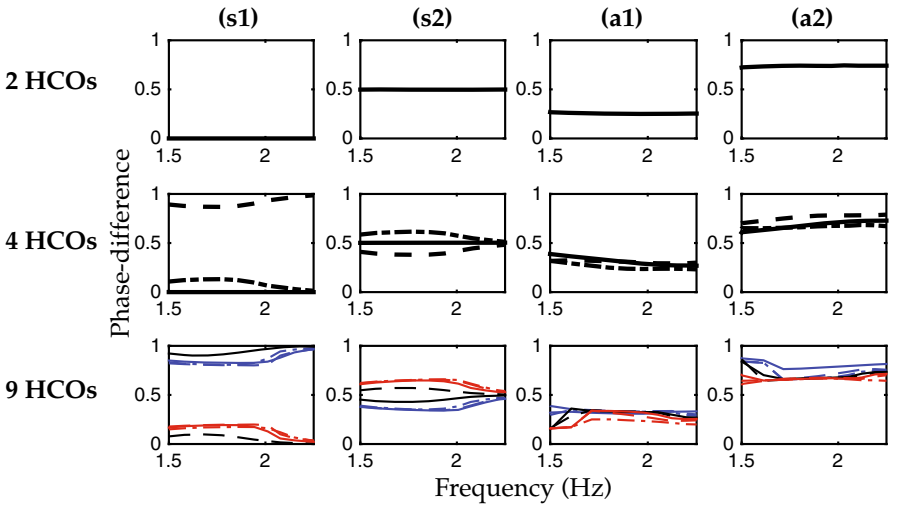

Fig. 4 The phase-difference(s) between neighboring pair(s) of HCOs in chains of 2, 4, and 9 HCOs, under the four fundamentally different inter-HCO connection topologies, as a function of the frequency of oscillation, respectively. The *four columns* correspond to the four inter-HCO connection topologies (*s1*), (*s2*), (*a1*), and (*a2*), respectively. Inter-HCO connection topologies are defined in Table 1 and illustrated in Fig. 3. *Top row (2-HCO chain)* The *solid black curve* shows the phase-difference as a function of the frequency of oscillation. *Middle row (4-HCO chain)* The *dashed black curve* shows the phase-difference between HCO-1 and HCO-2, the *solid black curve* shows the phase-difference between HCO-2 and HCO-3, and the *dashed-dotted curve* shows the phase-difference between HCO-3 and HCO-4, as functions of the frequency of oscillation. *Bottom row (9-HCO chain)* The *solid blue curve* shows the phase-difference between HCO-1 and HCO-2, the *dashed blue curve* shows the phase-difference between HCO-2 and HCO-3, the *dashed-dotted blue curve* shows the phase-difference between HCO-3 and HCO-4, the *solid black curve* shows the phase-difference between HCO-4 and HCO-5, the *dashed black curve* shows the phase-difference between HCO-5 and HCO-6, the *solid red curve* shows the phase-difference between HCO-6 and HCO-7, the *dashed red curve* shows the phase-difference between HCO-7 and HCO-8, and the *dashed-dotted red curve* shows the phase-difference between HCO-8 and HCO-9, as functions of the frequency of oscillation. (color figure online)

3.1 Coupled phase models of chains of HCOs

The coupled phase model is a commonly used mathematical framework for studying the dynamics of interconnected oscillators (Cohen et al. 1992; Williams et al. 1990; Kopell and Ermentrout 1988; Kuramoto 1984). In a phase model, the state of each oscillator is described completely by its phase θ_k, in which k is the index of the oscillator. If the k-th oscillator is isolated, then its phase θ_k evolves according to $d\theta_k/dt = \omega$, in which ω is the frequency of the isolated oscillator (i.e., the intrinsic period of oscillation is $T = 1/\omega$). If the k-th oscillator receives input from other oscillators, then the rate of change of its phase will speed up or slow down. The magnitude of the acceleration or deceleration of the phase of a perturbed oscillator depends on the timing and structure of the input from the presynaptic oscillators and on the state-dependent response of this postsynaptic oscillator. In a chain of oscillators with nearest-neighbor coupling, these effects are quantified by the ascending and descending *interaction functions*, H_{asc} and H_{dsc}, which are functions of the phase-difference

between the two inter-connected oscillators. Specifically, the phase of oscillator-k (θ_k) evolves according to the system of differential equations

$$\begin{cases} \dfrac{d\theta_1}{dt} = \omega + H_{\text{asc}}(\theta_2 - \theta_1), \\ \dfrac{d\theta_k}{dt} = \omega + H_{\text{asc}}(\theta_{k+1} - \theta_k) + H_{\text{dsc}}(\theta_{k-1} - \theta_k), \quad k = 2, \ldots, n-1, \\ \dfrac{d\theta_k}{dt} = \omega + H_{\text{dsc}}(\theta_{n-1} - \theta_n). \end{cases} \tag{12}$$

As a convention, the inter-oscillator connection from the $(k+1)$-th oscillator to the k-th oscillator is referred to as an *ascending* inter-HCO connection, and the inter-oscillator connection from the $(k-1)$-th oscillator to the k-th oscillator is referred to as a *descending* inter-HCO connection.

Two remarks are of importance here: (1) Because interaction functions are functions of the phase-difference, they are 1-periodic functions. (2) Each oscillatory unit is an HCO. That is, each oscillator is a "network oscillator", consisting of two neurons, or two neuronal populations, phase-locked in anti-phase. Thus, θ_k denotes the phase of the *entire* k-th HCO. This is a general feature of our model. Because each inter-oscillator connection originates from a particular neuron in the presynaptic HCO and terminates at a particular neuron in the postsynaptic HCO, the network topology of the inter-oscillator connections affects significantly the interaction functions.

Initially, for simplicity of discussion, we assume that the ascending and descending connections share the same strength and have the same synaptic properties, and that there is only one ascending and only one descending connection between each pair of neighboring HCOs. In Sect. 4, we will remove the above two constraints. Under these assumptions, the effect of the inter-HCO connection topology on the interaction function is captured by phase-shifts of a single interaction function H as follows

$$H_{\text{asc}}(\Delta\theta) = H(\Delta\theta + \phi_{\text{A}}), \tag{13}$$

$$H_{\text{dsc}}(\Delta\theta) = H(\Delta\theta + \phi_{\text{D}}), \tag{14}$$

in which $\Delta\theta$ is the phase-difference between two neighboring oscillators. The constant phase shifts, ϕ_{A} and ϕ_{D}, are determined by the inter-HCO connection topology. Recall that HCOs are composed of two mutually inhibitory internal neurons that oscillate in anti-phase, ϕ_{A} and ϕ_{D} take value of 0 or 0.5, depending on the neuron from which the inter-HCO connection originates and the neuron onto which the inter-HCO connection synapses. The values of ϕ_{A} and ϕ_{D} for the four fundamentally different inter-HCO connection topologies are listed in Table 1.

In terms of the phase-differences between neighboring oscillators $\Delta\theta_k = \theta_{k+1} - \theta_k$, the coupled phase model for a chain of HCOs is

$$\begin{cases} \dfrac{d\Delta\theta_1}{dt} = H(-\Delta\theta_1 + \phi_D) + H(\Delta\theta_2 + \phi_A) - H(\Delta\theta_1 + \phi_A), \\ \dfrac{d\Delta\theta_k}{dt} = H(-\Delta\theta_k + \phi_D) + H(\Delta\theta_{k+1} + \phi_A) - H(-\Delta\theta_{k-1} + \phi_D) - H(\Delta\theta_k + \phi_A) \\ \quad \text{for } k = 2, 3, \ldots, n-2, \ n \geq 3, \\ \dfrac{d\Delta\theta_{n-1}}{dt} = H(-\Delta\theta_{n-1} + \phi_D) - H(-\Delta\theta_{n-2} + \phi_D) - H(\Delta\theta_{n-1} + \phi_A). \end{cases} \tag{15}$$

Phase-locked states correspond to the solutions in which the inter-HCO phase-differences $\Delta\theta_k = \theta_{k+1} - \theta_k$ are constant:

$$\frac{d\Delta\theta_k}{dt} = 0, \quad \text{for } k = 1, 2, \ldots, n-1. \tag{16}$$

The existence of phase-locked states in chains of HCOs depends on the shape of the interaction function, which is determined by both the intrinsic properties of HCOs and the dynamical properties of the inter-oscillator coupling (Schwemmer and Lewis 2012).

3.2 The existence and stability conditions of four robust phase-waves

Perfect phase-waves are special phase-locked states in which the phase-differences $\Delta\theta_k$ are equal and constant for for all k, i.e., $(\Delta\theta_1, \Delta\theta_2, \ldots, \Delta\theta_{n-1}) = (\Delta\theta^*, \Delta\theta^*, \ldots, \Delta\theta^*)$ for some $0 \leq \Delta\theta^* < 1$. Our coupled phase model of chains of nearest-neighbor coupled HCOs (Eq. 15) captures both the internal mutually-inhibitory structure of the HCOs and the variety of inter-HCO connection topologies. Therefore, this model provides an appropriate framework to examine how these features influence the existence and stability of phase-waves.

3.2.1 Two coupled HCOs

We first consider a "chain" of two HCOs. In this case, our phase model (Eq. 15) reduces to a single differential equation that describes the evolution of the phase-difference between the two HCOs, $\Delta\theta = \theta_2 - \theta_1$,

$$\frac{d\Delta\theta}{dt} = H(-\Delta\theta + \phi_D) - H(\Delta\theta + \phi_A) =: G(\Delta\theta). \tag{17}$$

The condition for the existence of phase-locked states $\Delta\theta = \Delta\theta^*$ is

$$H(-\Delta\theta^* + \phi_D) - H(\Delta\theta^* + \phi_A) = G(\Delta\theta^*) = 0. \tag{18}$$

It can readily be seen that, under the two symmetric inter-HCO connection topologies (s1) and (s2) for which $\phi_D = 0, \phi_A = 0$ and $\phi_D = 0.5, \phi_A = 0.5$, respectively,

$$\Delta\theta^* = 0 \text{ and } 0.5 \tag{19}$$

are two *phase-constant* states (i.e., phase-locked states independent of the details of H).

Similarly,

$$\Delta\theta^* = 0.25 \text{ and } 0.75 \tag{20}$$

are two *phase-constant* states under the two asymmetric inter-HCO connection topologies (a1) and (a2) for which $\phi_D = 0.5, \phi_A = 0$ and $\phi_D = 0, \phi_A = 0.5$, respectively.

The stability of these phase-constant states depends on the sign of

$$G'(\Delta\theta^*) = -H'(-\Delta\theta^* + \phi_D) - H'(\Delta\theta^* + \phi_A). \tag{21}$$

The phase-locked state $\Delta\theta^*$ is stable if $G'(\Delta\theta^*) < 0$ and unstable if $G'(\Delta\theta^*) > 0$. For example, a stable phase-constant state at $\Delta\theta^* = 0$ (in-phase) under topology (s1) requires that $H'(0) > 0$, and this same phase-constant state under topology (s2) requires instead that $H'(0.5) > 0$.

Therefore, in a chain of two HCOs, symmetric inter-HCO connection topologies (s1) and (s2) *always* lead to the existence of the in-phase locking and the anti-phase locking, and asymmetric inter-HCO connection topologies (a1) and (a2) *always* lead to the existence of the 25 % phase-locking and the 75 % phase-locking. These four phase-locked states are robust in the sense that their existence is independent of the frequency of the oscillation and does not rely on tuning any specific biophysical parameters. The phase constancy of these four perfect phase-waves is a consequence of the particular organization of the inter-HCO connection topology.

3.2.2 A chain of n HCOs

The results for a pair of coupled HCOs can be extended to a chain of n HCOs with $n \geq 3$. Unlike the case for two HCOs, however, there are conditions on the interaction function H that need to be satisfied for *invariant* phase-waves to exist.

To see this, substituting $\Delta\theta_k = \Delta\theta^*(\ k = 1, 2, \ldots, n-1)$ into the steady state phase model equations (Eqs. 15, 16), we find that a perfect phase-wave with phase-differences $\Delta\theta^*$ exists if and only if

$$H(-\Delta\theta^* + \phi_D) = H(\Delta\theta^* + \phi_A) = 0. \tag{22}$$

The above equation consists of *two* separate constraints on H. With an appropriate inter-HCO connection topology, however, the above two constraints reduce to a *single* condition on H by ensuring $H(-\Delta\theta^* + \phi_D) = H(\Delta\theta^* + \phi_A)$:

1. Under topology (s1) for which $\phi_{\mathrm{D}} = 0$ and $\phi_{\mathrm{A}} = 0$, a phase-wave with $\Delta\theta^* = 0$ exists if and only if $H(0) = 0$, and a phase-wave with $\Delta\theta^* = 0.5$ exists if and only if $H(0.5) = 0$.
2. Under topology (s2) for which $\phi_{\mathrm{D}} = 0.5$ and $\phi_{\mathrm{A}} = 0.5$, a phase-wave with $\Delta\theta^* = 0$ exists if and only if $H(0.5) = 0$, and a phase-wave with $\Delta\theta^* = 0.5$ exists if and only if $H(0) = 0$.
3. Under topology (a1) for which $\phi_{\mathrm{D}} = 0.5$ and $\phi_{\mathrm{A}} = 0$, a phase-wave with $\Delta\theta^* = 0.25$ exists if and only if $H(0.25) = 0$, and a phase-wave with $\Delta\theta^* = 0.75$ exists if and only if $H(0.75) = 0$.
4. Under topology (a2) for which $\phi_{\mathrm{D}} = 0$ and $\phi_{\mathrm{A}} = 0.5$, a phase-wave with $\Delta\theta^* = 0.25$ exists if and only if $H(0.75) = 0$, and a phase-wave with $\Delta\theta^* = 0.75$ exists if and only if $H(0.25) = 0$.

Therefore, in chains of n HCOs with $n \geq 3$, a single condition on the interaction function H, determined by the inter-HCO connection topology, is necessary and sufficient to produce a phase-wave with $\Delta\theta^* = 0$, 25, 50, or 75 % in a robust manner independent of the frequency of oscillation. Without an appropriate inter-HCO connection topology such as those described in Table 1, multiple conditions on H would be required to ensure the existence of a phase-constant phase-wave.

3.2.3 Approximate phase-waves

In actual neuronal HCO networks, it would be too restrictive to enforce the exact condition on H (Eq. 22). Suppose $H(\Delta\theta^* + \phi_{\mathrm{A}})$ is not strictly equal to zero but close to zero, then one would expect the phase-locking to deviate by some small quantity dependent on the magnitude of $H(\Delta\theta^* + \phi_{\mathrm{A}})$. Motivated by this observation, we relax the condition on H by allowing the phase-differences in the phase-wave to deviate slightly from the perfect case $(\Delta\theta^*, \Delta\theta^*, \ldots, \Delta\theta^*)$ to be $(\Delta\theta_1^*, \Delta\theta_2^*, \ldots, \Delta\theta_{n-1}^*)$, where

$$\Delta\theta_k^* = \Delta\theta^* + d_k\epsilon + O(\epsilon^2), \qquad k = 1, 2, \ldots, n-1, \quad (n \geq 3) \tag{23}$$

in which ϵ is a small constant defined by

$$\epsilon = \frac{H(\Delta\theta^* + \phi_{\mathrm{A}})}{H'(\Delta\theta^* + \phi_{\mathrm{A}})}, \tag{24}$$

and d_k are coefficients in the order of $O(1)$ to be determined by the length of the HCO chain. That is, to first order in ϵ, we have assumed that there is a small linear gradient in the phase-differences down the chain of HCOs. In the following, we refer to this perturbed phase-wave with phase-differences $(\Delta\theta_1^*, \Delta\theta_2^*, \ldots, \Delta\theta_{n-1}^*)$ as the *approximate $\Delta\theta^*$ phase-wave*. Note that the approximate phase-wave reduces to the perfect phase-wave case if $\epsilon = 0$.

Table 2 The existence conditions for the four approximate $\Delta\theta^*$ phase-waves in chains of n HCOs ($n \geq 3$) under the four fundamentally different inter-HCO connection topologies

$\Delta\theta^*$	Topology (s1)	Topology (s2)	Topology (a1)	Topology (a2)
In-phase (0 %)	$\frac{(n-2)H(0)}{nH'(0)}$ is small	$\frac{(n-2)H(0.5)}{nH'(0.5)}$ is small	Not robust	Not robust
25 %	Not robust	Not robust	$\frac{(n-2)H(0.25)}{nH'(0.25)}$ is small	$\frac{(n-2)H(0.75)}{nH'(0.75)}$ is small
Anti-phase (50 %)	$\frac{(n-2)H(0.5)}{nH'(0.5)}$ is small	$\frac{(n-2)H(0)}{nH'(0)}$ is small	Not robust	Not robust
75 %	Not robust	Not robust	$\frac{(n-2)H(0.75)}{nH'(0.75)}$ is small	$\frac{(n-2)H(0.25)}{nH'(0.25)}$ is small

Note that in the case $n = 2$, the existence is unconditional under appropriate inter-HCO connection topology (see text and Zhang et al. (2014) for the $n = 2$ case)

To determine d_k, we plug the approximate phase-wave (Eq. 23) into the steady state phase model equations (Eqs. 15, 16). To first order in ϵ, we obtain

$$\begin{cases} (1-d_1)H(-\Delta\theta^*+\phi_D)+(1+d_2)H(\Delta\theta^*+\phi_A)-(1+d_1)H(\Delta\theta^*+\phi_A)=0, \\ (1-d_k)H(-\Delta\theta^*+\phi_D)+(1+d_{k+1})H(\Delta\theta^*+\phi_A)- \\ \qquad (1-d_{k-1})H(-\Delta\theta^*+\phi_D)-(1+d_k)H(\Delta\theta^*+\phi_A)=0, \\ \quad \text{for } k=2,3,\ldots,n-2, \quad (n\geq 3) \\ (1-d_{n-1})H(-\Delta\theta^*+\phi_D)-(1-d_{n-2})H(-\Delta\theta^*+\phi_D)-(1+d_{n-1})H(\Delta\theta^*+\phi_A)=0. \end{cases} \tag{25}$$

Recall that with an appropriate inter-HCO connection topology described in Table 1, we have

$$H(\Delta\theta^*+\phi_A)=H(-\Delta\theta^*+\phi_D). \tag{26}$$

Solving Eq. 25 for d_k, we obtain

$$d_k=\frac{n-2k}{n}, \quad \text{for } k=1,2,\ldots,n-1. \tag{27}$$

Hence, the phase-differences in the approximate $\Delta\theta^*$ phase-wave defined in Eq. 23 can be rewritten as

$$\Delta\theta_k^*=\Delta\theta^*+\frac{n-2k}{n}\epsilon+O(\epsilon^2), \qquad k=1,2,\ldots,n-1. \tag{28}$$

The complete results for different inter-HCO connection topologies are listed in Table 2. For example, if $n = 4$, under topology (a1), the approximate 25% phase-wave is $(\Delta\theta_1^*, \Delta\theta_2^*, \Delta\theta_3^*) = (0.25+\epsilon/2, 0.25, 0.25-\epsilon/2)$ where $\epsilon = H(0.25)/H'(0.25)$.

3.2.4 Stability

The stability of an approximate or perfect phase-wave depends on the eigenvalues of the Jacobian matrix of the right-hand-side of Eq. 15

$$J(\epsilon) = \begin{pmatrix} -s_{\mathrm{D}}^{(1)} - s_{\mathrm{A}}^{(1)} & s_{\mathrm{A}}^{(2)} & & & & \\ s_{\mathrm{D}}^{(1)} & -s_{\mathrm{D}}^{(2)} - s_{\mathrm{A}}^{(2)} & s_{\mathrm{A}}^{(3)} & & & \\ & \ddots & \ddots & \ddots & & \\ & & s_{\mathrm{D}}^{(n-3)} & -s_{\mathrm{D}}^{(n-2)} - s_{\mathrm{A}}^{(n-2)} & s_{\mathrm{A}}^{(n-1)} & \\ & & & s_{\mathrm{D}}^{(n-2)} & -s_{\mathrm{D}}^{(n-1)} - s_{\mathrm{A}}^{(n-1)} & \end{pmatrix}, \tag{29}$$

in which $s_{\mathrm{D}}^{(k)} = H'(-\Delta\theta^* + \phi_{\mathrm{D}} - \frac{n-2k}{n}\epsilon + O(\epsilon^2))$ and $s_{\mathrm{A}}^{(k)} = H'(\Delta\theta^* + \phi_{\mathrm{A}} + \frac{n-2k}{n}\epsilon + O(\epsilon^2))$ for $k = 1, 2, \ldots, n-1$. The phase-wave is stable if all eigenvalues of $J(\epsilon)$ have negative real parts and is unstable if at least one of the eigenvalues of $J(\epsilon)$ has positive real part. Note that, because $|\epsilon| \ll 1$, the signs of the real part of the eigenvalues of $J(\epsilon)$ are inherited from the eigenvalues of $J(0)$, which is the Jacobian matrix corresponding to the system with the perfect phase-wave ($\epsilon = 0$).

With an appropriate network topology for the $\Delta\theta^*$ phase-wave ($\Delta\theta^* = 0$, 0.25, 0.5 or 0.75), the Jacobian matrix reduces to

$$J(0) = H'(\Delta\theta^* + \phi_{\mathrm{A}}) \begin{pmatrix} -2 & 1 & & & \\ 1 & -2 & 1 & & \\ & \ddots & \ddots & \ddots & \\ & & 1 & -2 & 1 \\ & & & 1 & -2 \end{pmatrix}. \tag{30}$$

Therefore, the stability of the phase-wave is determined by the sign of $H'(\Delta\theta^* + \phi_{\mathrm{A}})$. For example, under connection topology (s1), in-phase locking ($\Delta\theta^* = 0$) is stable if $H'(0) > 0$, and under connection topology (s2), in-phase locking is stable if $H'(0.5) > 0$. Under connection topology (a1), the $\Delta\theta^* = 0.25$ phase-wave is stable if $H'(0.25) > 0$, and under connection topology (a2), the $\Delta\theta^* = 0.25$ phase-wave is stable if $H'(0.75) > 0$. The complete stability results for different inter-HCO connection topologies are listed in Table 3.

3.2.5 Summary

The existence and stability conditions of the four robust $\Delta\theta^*$ phase-waves under the four fundamentally different inter-HCO connection topologies are summarized in Tables 2 and 3, respectively. In the case $n = 2$, the existence of these four robust phase waves is independent of the details of H and is solely a result of the inter-HCO connection topology. In cases of chains of n HCOs with $n \geq 3$, the condition $H(\Delta\theta^* + \phi_{\mathrm{A}}) = 0$ needs to be satisfied. This is because the HCOs on the ends of the chain receive a different number of synaptic inputs than the HCOs in the middle

Table 3 Stability conditions for the four approximate $\Delta\theta^*$ phase-waves in chains of n HCOs ($n \geq 3$) under the four fundamentally different inter-HCO connection topologies

$\Delta\theta^*$	Topology (s1)	Topology (s2)	Topology (a1)	Topology (a2)
In-phase (0 %)	$H'(0) > 0$	$H'(0.5) > 0$	Not robust	Not robust
25 %	Not robust	Not robust	$H'(0.25) > 0$	$H'(0.75) > 0$
Anti-phase (50 %)	$H'(0.5) > 0$	$H'(0) > 0$	Not robust	Not robust
75 %	Not robust	Not robust	$H'(0.75) > 0$	$H'(0.25) > 0$

Note that the same stability conditions applies to the case $n = 2$, in which the chain of two HCOs produces the perfect $\Delta\theta^*$ phase-wave (see text and Zhang et al. (2014) for the $n = 2$ case)

of the chain. This end effect breaks the symmetry that existed in the case of $n = 2$. Nevertheless, because of the special organization of the four inter-HCO connection topologies, a chain of HCOs with $n \geq 3$ only needs to meet one condition in order to produce one of the four robust phase-waves with approximate phase-differences at 0%, 25%, 50%, or 75%. Without an appropriate inter-HCO connection topology, more than one conditions on H would be required.

4 Variations in inter-HCO connections

In this section, we extend the results of the previous section to chains of nearest-neighbor coupled HCOs to allow variations in the strength and the number of inter-HCO connections. Specifically, we show that an approximate 0, 25, 50, or 75 % phase-waves persists (1) regardless of the difference in strength between the ascending and descending connections, and (2) in the presence of multiple nearest-neighbor inter-HCO connections as long as the fundamental inter-HCO connection topology is preserved.

4.1 Inter-HCO connections with unequal strengths between the ascending and descending directions

To consider a difference in strengths between the ascending and descending inter-HCO connections, we redefine the interaction functions of the ascending and descending connections by

$$H_{\text{asc}}(\Delta\theta_k) = \alpha H(\Delta\theta_k + \phi_{\text{A}}), \tag{31}$$

$$H_{\text{dsc}}(-\Delta\theta_k) = \beta H(-\Delta\theta_k + \phi_{\text{D}}), \tag{32}$$

in which α and β are numbers with the same sign that determine the strengths of the ascending and the descending connections, respectively, and ϕ_{A} and ϕ_{D} are as defined previously. We take the ratio of the ascending to descending connection strengths

$$a = \frac{\alpha}{\beta} \tag{33}$$

as our measure of the level of heterogeneity.

With $a \neq 1$, we expect the phase-differences in the perfect Δ^* phase-wave to deviate from $(\Delta\theta^*, \Delta\theta^*, \ldots, \Delta\theta^*)$. We denote the phase-differences in the resulting approximate phase-wave by

$$\begin{aligned}&(\Delta\theta_1, \Delta\theta_2, \ldots, \Delta\theta_{n-1})\\ &= (\Delta\theta^* + e_1\epsilon + O(\epsilon^2),\ \Delta\theta^* + e_2\epsilon + O(\epsilon^2),\ \ldots,\ \Delta\theta^* + e_{n-1}\epsilon + O(\epsilon^2)),\end{aligned} \tag{34}$$

in which e_k are coefficients in the order of $O(1)$ to be determined, and ϵ is a small constant that measures the imperfection of the zero of the interaction function H as previously defined in Eq. 24. Substituting this approximate phase-wave for the phase-differences in the steady state phase model equations (Eqs. 15, 16), we obtain, to first order in ϵ,

$$\begin{cases}(a+1)e_1 - ae_2 - 1 = 0,\\ e_{k-1} - (a+1)e_k + ae_{k+1} = 0 \quad \text{for } k = 2, 3, \ldots, n-2\ (n \geq 3),\\ e_{n-2} - (a+1)e_{n-1} - a = 0.\end{cases} \tag{35}$$

Solving the above equation for the coefficients e_k, we obtain

$$e_k = \frac{a^n - 2a^{n-k} + 1}{1 - a^n}, \quad \text{for } k = 1, 2, \ldots, n-1. \tag{36}$$

$e_k\epsilon$ quantifies the first order effect of the ratio of the ascending to descending connection strengths, a, on the inter-HCO phase-differences. Equation 36 shows that, as $a \to 1$ (i.e., equal ascending and descending connection strengths), e_k reduces to d_k (Eq. 27) as described in the previous subsection. More importantly, it shows that $e_k = O(1)$ for all $a \geq 0$. Therefore, deviations away from the perfect phase-wave are small for any ascending to descending strength ratio.

Figure 5 plots e_k for a chain of 10 HCOs with various values of a. When $a = 1$, there is a small linear decrease in e_k from $k = 1$ to $k = 9$ (i.e., assuming $\epsilon > 0$, there is a small decrease in phase-difference down the chain). When $a > 1$, e_k is concave up, and approaches -1 as k increases. When $a < 1$, e_k is concave down, and approaches 1 as k decreases. When a is small (i.e., descending connections dominate) or when a is large (i.e., ascending connections dominate), $e_k \approx 1$ or $e_k \approx -1$ for all k except at one end of the chain. The above results are obtained under the phase-HCO model. Similar results are also obtained under the conductance-based ML-HCO model. (See the Appendix for figures showing the the phase-differences between neighboring pair of HCOs in a chain of 10 HCOs under the four different inter-HCO connection topologies.) This implies that, if only ascending or only descending connections are present, near perfect phase-waves exist with only small boundary effects.

The functional significance of the above results is that regardless of the ratio of the ascending to descending connection strengths, the deviation of the phase-differences is always in the order of $O(\epsilon)$, and therefore an asymmetry in the ascending and descending inter-HCO connection strength does not affect the existence of the four robust approximate phase-waves.

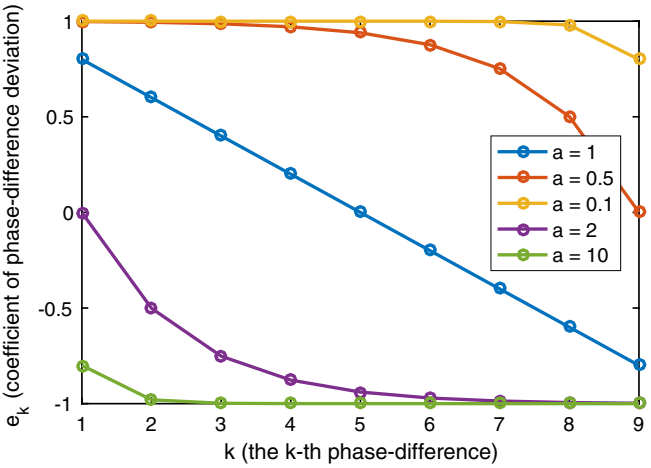

Fig. 5 The effect of the difference in the synaptic strength between the ascending and descending inter-HCO connections on the phase-differences in a chain of 10 HCOs with nearest-neighbor coupling. The coefficient of the deviation of the phase-differences e_k (Eq. 36) is plotted as a function of k, $k = 1, 2, \ldots, 9$ for four different values of $a = \alpha/\beta$, where α and β are the strength of the ascending and descending connections, respectively (color figure online)

4.2 Multiple inter-HCO connections between neighboring HCOs

There are 8 possible inter-HCO connections between each pair of neighboring HCOs: 4 different ascending connections and 4 different descending connections. Define $H_{\text{asc}}(\Delta\theta) = H(\Delta\theta)$ to be the interaction function for the ascending connection from Neuron 1 to Neuron 1, and $H_{\text{dsc}}(-\Delta\theta)$ to be the interaction function for the descending connection from Neuron 1 to Neuron 1. Then, accounting for the anti-phase activity in the HCOs and again assuming homogeneous synaptic dynamics and response properties of neurons, the coupled phase model for chains of nearest-neighbor coupled n HCOs with all eight possible inter-HCO connections is given by

$$\begin{cases} \dfrac{d\theta_1}{dt} = \omega + (\alpha_{2\to2} + \alpha_{1\to1})H(\Delta\theta_1) + (\alpha_{2\to1} + \alpha_{1\to2})H(\Delta\theta_1 + 0.5), \\ \dfrac{d\theta_i}{dt} = \omega + (\alpha_{2\to2} + \alpha_{1\to1})H(\Delta\theta_i) + (\alpha_{2\to1} + \alpha_{1\to2})H(\Delta\theta_i + 0.5) \\ \qquad\quad + (\beta_{2\to2} + \beta_{1\to1})H(-\Delta\theta_{i-1}) + (\beta_{2\to1} + \beta_{1\to2})H(-\Delta\theta_{i-1} + 0.5), \\ \qquad\quad \text{for } i = 2, 3, \ldots, n-1, \\ \dfrac{d\theta_n}{dt} = \omega + (\beta_{2\to2} + \beta_{1\to1})H(-\Delta\theta_{n-1}) + (\beta_{2\to1} + \alpha_{1\to2})H(-\Delta\theta_{n-1} + 0.5), \end{cases} \tag{37}$$

in which ω is the intrinsic frequency of the HCOs, $\Delta\theta_i = \theta_{i+1} - \theta_i$ is the phase-difference between each pair of neighboring HCOs, $\alpha_{\text{i}\to\text{j}}$ is the strength of the ascending connection from Neuron i to Neuron j, and $\beta_{\text{i}\to\text{j}}$ is the strength of the descending connection from Neuron i to Neuron j ($i, j = 1, 2$).

It follows that a perfect phase-wave $(\Delta\theta^*, \Delta\theta^*, \ldots, \Delta\theta^*)$ exists if and only if

$$\begin{cases} (\alpha_{2\to 2} + \alpha_{1\to 1})H(\Delta\theta^*) + (\alpha_{2\to 1} + \alpha_{1\to 2})H(\Delta\theta^* + 0.5) = 0, \\ (\beta_{2\to 2} + \beta_{1\to 1})H(-\Delta\theta^*) + (\beta_{2\to 1} + \beta_{1\to 2})H(-\Delta\theta^* + 0.5) = 0. \end{cases} \tag{38}$$

For phase-waves to exist with a single condition on the interaction function H (as in Sect. 3), restrictions on the inter-HCO connections are required. For example, if $H(0) = 0$ and there are no other restrictions on H, then the in-phase locking $\Delta\theta^* = 0$ exists if and only if $\beta_{2\to 1} + \beta_{1\to 2} = 0$ and $\alpha_{2\to 1} + \alpha_{1\to 2} = 0$. Assuming that all synaptic connections are excitatory (or inhibitory), i.e., α's and β's are non-negative (or non-positive), this condition corresponds to the case in which there are no cross connections. In other words, the ascending and descending connections must be parallel, such as from Neuron 1 to Neuron 1, or from Neuron 2 to Neuron 2. This implies that the generalized version of inter-HCO connection topology (s1) described in Table 1 removes the condition that $H(0.5) = 0$ for the existence of the in-phase state, which is stable if

$$(\beta_{2\to 2} + \beta_{1\to 1} + \alpha_{2\to 2} + \alpha_{1\to 1})H'(0) > 0. \tag{39}$$

As another example, if $H(0.25) = 0$ and there are no other restrictions on H, then the phase-wave with $\Delta\theta^* = 0.25$ exists if and only if $\beta_{2\to 2} + \beta_{1\to 1} = 0$ and $\alpha_{2\to 1} + \alpha_{1\to 2} = 0$. Under the assumption that all synaptic connections are excitatory (or inhibitory), this condition corresponds to the case in which the descending connection must be cross connections, such as from Neuron 1 to Neuron 2, or from Neuron 2 to Neuron 1, whereas the ascending connections must be parallel, such as from Neuron 1 to Neuron 1, or from Neuron 2 to Neuron 2. This implies that the generalized version of the inter-HCO coupling topology (a1) described in Table 1 removes the condition that $H(0.75) = 0$. The phase-wave with 25 % inter-HCO phase-difference is stable if

$$(\beta_{2\to 1} + \beta_{1\to 2} + \alpha_{2\to 2} + \alpha_{1\to 1})H'(0.25) > 0. \tag{40}$$

The incorporation of appropriate inter-HCO connections does not change the fundamental mechanism producing the robust phase-waves. Connectivity schemes that utilize a symmetric ascending/descending inter-HCO connection topology are able to produce robust in-phase or anti-phase phase-wave in the sense that only one constraint on the response properties of the HCO (that is, the condition that $H(\Delta\theta^*) = 0$ or $H(\Delta\theta^* + 0.5) = 0$) is required. On the other hand, connectivity schemes that utilize an asymmetric ascending/descending inter-HCO connection topology are able to produce robust 25 or 75 % phase-wave with only one constraint on the response properties of the HCO. As long as the additional inter-HCO connections maintain the same inter-HCO connection topology, then one of the four phase-waves with phase-differences at 0, 25, 50, or 75 % still arises robustly via the same mechanism we have discussed in the previous section.

5 Robust phase-waves in rings of HCOs

As shown in Sect. 3, for a perfect phase-wave to exist in a chain of three or more HCOs, the interaction function H of the HCOs is required to have a zero at a particular phase-difference, or for an approximate phase-wave to exist, H/H' is required to be small near that particular phase-difference, i.e., $|\epsilon| \ll 1$. This requirement arises because the HCOs at the ends of the chain receive *only* ascending input *or* descending input whereas all other HCOs receive *both* ascending input *and* descending input. That is, symmetry is broken at the ends of the chain when the number of HCOs is three or more. This "end effect" is the cause of the slight deviation in phase-lags along the chain of three or more HCOs. This symmetry can be restored if a ring of HCOs is formed by connecting HCOs at the ends of the chain with the same inter-HCO connection topology as the neighboring pairs of HCOs in the middle of the chain. In this section, we determine conditions for the existence and stability of phase-waves in rings of HCOs and contrast them to the conditions for phase-waves in chains of HCOs. We analyze the rings of HCOs to emphasize the fundamental difference between the existence of robust phase-waves in chains of HCOs and in rings of HCOs.

The phase-differences of neighboring HCOs in a ring of nearest-neighbor, bi-directionally coupled HCOs are given by

$$\frac{d\theta_k}{dt} = \omega + H_{\text{asc}}(\theta_{k+1} - \theta_k) + H_{\text{dsc}}(\theta_{k-1} - \theta_k), \tag{41}$$

for $k = 1, 2, \ldots, n$ with conditions for periodicity $\theta_0 = \theta_n$ and $\theta_{n+1} = \theta_1$. In terms of phase-differences $\Delta\theta_k = \theta_{k+1} - \theta_k$, we have

$$\frac{d\,\Delta\theta_k}{dt} = H_{\text{dsc}}(-\Delta\theta_k) + H_{\text{asc}}(\Delta\theta_{k+1}) - H_{\text{dsc}}(-\Delta\theta_{k-1}) - H_{\text{asc}}(\Delta\theta_k), \tag{42}$$

for $k = 1, 2, \ldots, n-1$ with conditions for periodicity $\Delta\theta_0 = \theta_1 - \theta_n$ and $\Delta\theta_n = \theta_1 - \theta_n$. Note that these conditions for periodicity imply that

$$\Delta\theta_n = \theta_1 - \theta_n = \sum_{k=1}^{n-1}(\theta_k - \theta_{k+1}) = -\sum_{k=1}^{n-1}\Delta\theta_k, \tag{43}$$

or

$$\sum_{k=1}^{n}\Delta\theta_k \mod 1 = 0. \tag{44}$$

For a perfect (rotating) phase-wave $\Delta\theta_k = \Delta\theta^*(k = 1, 2, \ldots, n-1)$ to exist, it must satisfy both the steady state equations of Eq. 42 and the periodicity condition Eq. 44. Using the same convention that was used in the analysis of the n-HCO chain, that is, $H_{\text{asc}}(\Delta\theta) = H(\Delta\theta + \phi_{\text{A}})$ and $H_{\text{dsc}}(\Delta\theta) = H(\Delta\theta + \phi_{\text{D}})$, in which ϕ_{D} and ϕ_{A} are determined by the inter-HCO connection topology (see Table 1), the right-hand-sides of the steady state equations of Eq. 42 are *always* zero! Thus, perfect phase-waves

exist if and only if the periodicity condition Eq. 44 is satisfied, i.e., whenever

$$\Delta\theta^* = \frac{j}{n}, \quad \text{for } j = 0, 1, 2 \ldots, n-1. \tag{45}$$

The stability of the $\Delta\theta^* = j/n$ phase-wave in a ring of HCOs depends on the eigenvalues of the Jacobian matrix of the right-hand-side of Eq. 42

$$J_{\text{ring}} = \begin{pmatrix} -2s_D - s_A & s_A - s_D & -s_D & -s_D & -s_D \\ s_D & -s_D - s_A & s_A & & \\ & \ddots & \ddots & \ddots & \\ & & s_D & -s_D - s_A & s_A \\ -s_A & -s_A & -s_A & s_D - s_A & -s_D - 2s_A \end{pmatrix}, \tag{46}$$

in which $s_D = H'(-j/n + \phi_D)$, $s_A = H'(j/n + \phi_A)$. One can show that if

$$H'(-j/n + \phi_D) + H'(j/n + \phi_A) > 0, \tag{47}$$

then all eigenvalues of J_{ring} have negative real parts. Therefore, the j/n phase-wave ($j = 0, 1, 2, \ldots, n-1$) is stable if $H'(-j/n + \phi_D) + H'(j/n + \phi_A) > 0$.

It is important to emphasize the fundamental difference between the existence of *robust* phase-waves in chains of HCOs and in rings of HCOs. For a chain of n-HCOs, there exists only two robust phase-waves with inter-HCO phase-differences of either 0 and 50 %, or 25 and 75 %, and these phase-waves depend on both the internal structure of the HCOs and network topology of the inter-HCO coupling. On the other hand, for a ring of n-HCOs, there exists n phase-waves with inter-HCO phase-differences that depend on n, and the existence of these phase-waves is independent of both the internal structure of the HCO and the connection topology between HCOs (as long as the inter-HCO connectivity is the same between each neighboring pair of HCOs in either coupling direction). Note that this latter result is similar to a more general result for rings in (Ermentrout 1985).

6 Discussion

In this article, we have shown how the internal anti-phase structure of the HCO and the inter-HCO connection topology combine to promote robust (i.e., phase-constant) phase-waves in chains of HCOs with nearest-neighbor coupling. Specifically, under the framework of the coupled phase model with the full HCOs as the oscillating units, we have derived conditions for the *robust* existence and stability of phase-waves with inter-HCO phase-differences $\Delta\theta^* = 0$, 25, 50, or 75 % under four fundamentally different inter-HCO connection topologies. For a pair of HCOs, a robust $\Delta\theta^*$ phase-locking exists independently of the interaction function H and therefore independently of the frequency of oscillation (and all the biophysical details) of the HCO. In general, the existence of a robust phase-wave in a chain of three or more HCOs would require multiple conditions on H, but appropriate inter-HCO connection topologies reduce this

requirement to a single condition in the form of either $H(\Delta\theta^*) \approx 0$ or $H(\Delta\theta^*+0.5) \approx 0$. The value of $\Delta\theta^*$ is determined by the inter-HCO connection topology.

The conditions for robust phase-waves described here can help identify the mechanisms that give rise to phase-constancy in some locomotor systems but not in others. The neural circuit underlying limb coordination in the crayfish swimmeret system has been shown to consists of a chain of four HCOs with the (a1) inter-HCO connection topology (Zhang et al. 2014; Smarandache-Wellmann et al. 2014). Because our results link the (a1) connection topology to the robust existence of the 25 % phase-wave, they explain how the circuit architecture helps to maintain the frequency-independent approximate 25 % phase-differences between swimmerets of crayfish and other long-tailed crustaceans during forward swimming. Similarly, locomotor neural circuits in stick insects and cockroaches are well-modeled by chains of HCOs with symmetric inter-HCO coupling (Daun-Gruhn and Toth 2011; Proctor et al. 2010), and thus our results also can help explain the robustness of the tripod gait of insects, which is characterized by the phase-constant rhythm with approximate 50% inter-limb phase-differences. On the other hand, the mechanisms described here do not apply to gait transitions, which likely involve significant changes in the interaction function H or bistability between different phase-waves. Furthermore, although the neural circuits underlying the body motion during undulatory swimming of lamprey and leech consist of chains of HCOs (Sigvardt and Miller 1974; Kristan et al. 1974), our results do not explain the corresponding 1 and 3 % phase-waves in these systems. These cases and other cases that have phase-lags different from 0, 25, 50, or 75 % likely employ more subtle mechanisms, involving well-tuned compensatory mechanisms that maintain the zeros of the interaction function H at the appropriate value, the effects of long-range coupling, and/or more complex network structures.

The work presented here fits between previous work on phase-locking in chains of generic phase oscillators and work that employs symmetry arguments to account for robust phase-locking. Much of the extensive work on phase-locking in chains of coupled generic phase oscillators focuses on identifying conditions on the interaction function H for the existence of phase-waves [e.g., Cohen and Kiemel (1993), Kopell and Ermentrout (1986)]. In fact, Skinner et al. (1997) specifically derived conditions on H for the existence of a 25 % phase wave for a chain of four oscillators in the context of the crayfish swimmeret system. We have extended this work by generalizing it and linking directly the constraints on H to the architecture of the neural circuit.

Symmetry arguments have been used to show that robust phase-locking in networks of oscillators can arise solely from the type and topology of coupling between units rather than from any well-tuned intrinsic mechanism of the local oscillators or synaptic dynamics [e.g., Golubitsky et al. (1999), Collins and Stewart (1993)] . These symmetry arguments cannot be applied directly to chains of HCOs (or even to most of the pairs of HCOs considered in this article) because chains of HCOs do not have the appropriate level of symmetry. However, symmetry arguments can still be used to reduce the number of constraints for the robust existence of phase-waves given the appropriate assumptions. By exploiting the strong coupling between the two internal neurons of each HCO and the relatively weak inter-HCO coupling, a

chain of HCOs can be reduced to a chain of phase oscillators in which each HCO is an oscillatory unit with a single phase but with two possible output and input pathways that are shifted by half of a period. Even with the chain of phase oscillators (beyond pairs), symmetry arguments cannot be applied directly because the oscillators at the ends of the chain receive a different number of inputs than those oscillators in the middle of the chain. Nevertheless, the symmetry between individual pairs of HCOs along the chain decreases the requirements to produce robust phase-locking to a single constraint, which comes in the form of a condition of the H-function.

Changes in the frequency of oscillators usually lead to changes in the shape of the interaction function H and shifts the zeros of the H function; this in turn will alter the phase-differences in a chain of oscillators. However, as mentioned above, for a chain of HCO to exhibit phase-constancy, the zeros of H must remain approximately fixed. In the case of the crayfish swimmeret system, experimentally-derived H functions for the local CPGs have zeroes close to 25 % for arbitrary frequencies (Zhang et al. 2014; Smarandache-Wellmann et al. 2014). This taken together with the facts that the crayfish swimmeret CPGs are HCOs and that the inter-HCO connections are asymmetric provides a mechanism for generating the phase-constant phase-waves with 25 % inter-segmental phase-differences in the swimmeret system. Furthermore, in (Zhang et al. 2014), we have recently shown that the phase response properties of idealized HCOs (based on the Wang-Rinzel (Wang and Rinzel 1992) or the Morris–Lecar (Skinner et al. 1994) HCO model) are able to produce H functions in which the zeroes are close to 25 and 75 % largely independent of the frequency of oscillation. Future work is needed to further elucidate how the interaction functions are shaped by the underlying dynamics of CPGs and the inter-CPG synaptic dynamics (Zhang and Lewis 2013) and satisfy requirement for robust phase-waves.

Acknowledgements CZ and TJL were partially supported by NSF under grant number CRCNS 0905063. CZ is a Courant Instructor.

Appendix: Numerical results of the ML-HCO model: inter-HCO connections with unequal strengths between the ascending and descending directions

In Sect. 4.1, we used the phase-HCO model to show that an approximate 0, 25, 50, or 75 % phase-waves persists regardless of the difference in strength between the ascending and descending connections. Here, we verify the above result using the conductance-based ML-HCO model. We consider a chain of 10 HCOs under the four fundamentally different inter-HCO connection topologies. Figures 6, 7, 8, 9 show that regardless of the ratio of the ascending to descending connection strengths, the deviation of the phase-differences is always in the order of $O(\epsilon)$ (see Eq. 24 for definition of ϵ). Both the phase-HCO model and the ML-HCO model give the same result that an asymmetry in the ascending and descending inter-HCO connection strength does not affect the existence of the four robust approximate phase-waves.

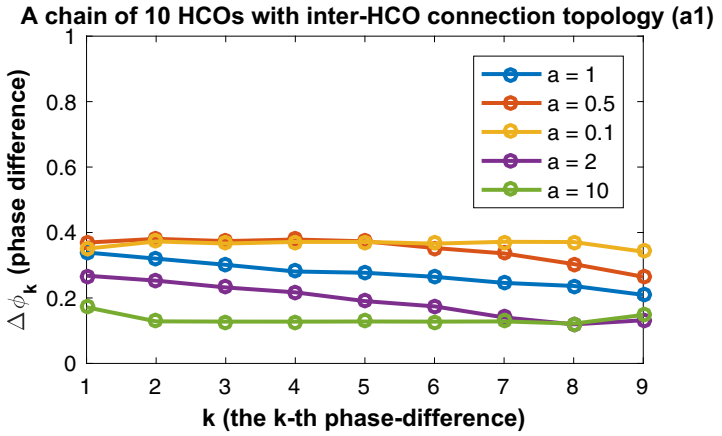

Fig. 6 The effect of the difference in the synaptic strength between the ascending and descending inter-HCO connections on the phase-differences in a chain of 10 HCOs with inter-HCO connection topology (*a1*). The phase-differences $\Delta\phi_k$ (Eq. 36) is plotted as a function of k, $k = 1, 2, \ldots, 9$ for four different values of $a = \alpha/\beta$, where α and β are the strength of the ascending and descending connections, respectively. Numerical simulation of this ML-HCO model was performed using the same parameters reported in Sect. 2 (color figure online)

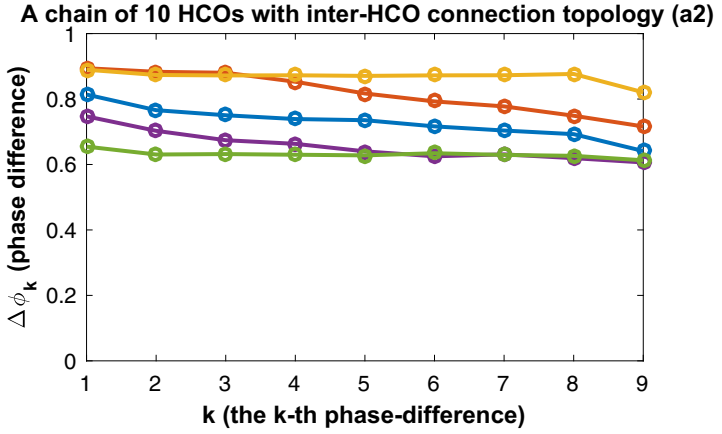

Fig. 7 The effect of the difference in the synaptic strength between the ascending and descending inter-HCO connections on the phase-differences in a chain of 10 HCOs with inter-HCO connection topology (*a2*). See the caption and legend of Fig. 6 for descriptions (color figure online)

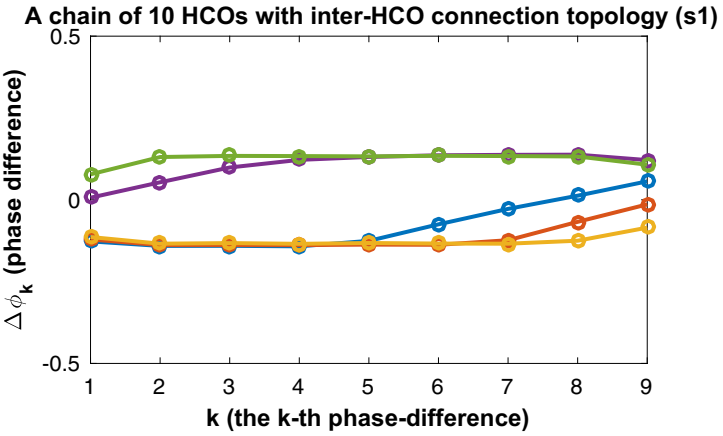

Fig. 8 The effect of the difference in the synaptic strength between the ascending and descending inter-HCO connections on the phase-differences in a chain of 10 HCOs with inter-HCO connection topology (*s1*). See the caption and legend of Fig. 6 for descriptions (color figure online)

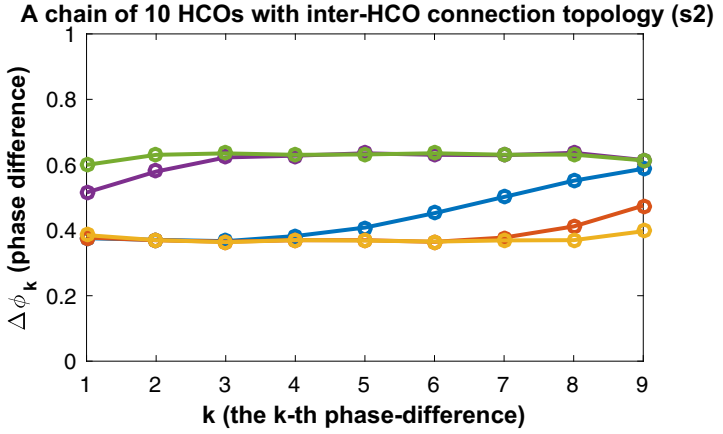

Fig. 9 The effect of the difference in the synaptic strength between the ascending and descending inter-HCO connections on the phase-differences in a chain of 10 HCOs with inter-HCO connection topology (*s2*). See the caption and legend of Fig. 6 for descriptions (color figure online)

References

Chevalliera S, Ijspeertb AJ, Ryczkoa D, Nagya F, Cabelguen JM (2008) Organisation of the spinal central pattern generators for locomotion in the salamander: Biology and modelling. Brain Res Rev 57:147–161

Clewley R (2011) Inferring and quantifying the role of an intrinsic current in a mechanism for a half-center bursting oscillation. J Biol Phys 37:285–306

Cohen AH, Ermentrout GB, Kiemel T, Kopell N, Sigvardt KA, Williams TL (1992) Modeling of intersegmental coordination in the lamprey central pattern generator for locomotion. Trends Neurosci 15:434–438

Cohen AH, Holmes PJ, Rand RH (1982) The nature of the coupling between segmental oscillators of the lamprey spinal generator for locomotion: A mathematical model. J Math Biol 13:345–369

Cohen AH, Kiemel T (1993) Intersegmental coordination: lessons from modeling systems of coupled nonlinear oscilaltors. Am Zool 33:54–65
Collins JJ, Stewart I (1993) Coupled nonlinear oscillators and the symmetries of animal gaits. J Nonlinear Sci 3:349–392
Daun-Gruhn S, Toth TI (2011) An inter-segmental network model and its use in elucidating gait-switches in the stick insect. J Comput Neurosci 31:43–60
Ermentrout GB (1985) The behavior of rings of coupled oscillators. J Math Biol 23:55–74
Golubitsky M, Stewart I, Buono PL, Collins JJ (1999) Symmetry in locomotor central pattern generators and animal gaits. Nature 401:693–695
Grillner S (2006) Biological pattern generation: the cellular and computational logic of networks in motion. Neuron 52:751–766
Hill AA, Masino MA, Calabrese RL (2003) Intersegmental coordination of rhythmic motor patterns. J Neurophysiol 90:531–538
Hooper SL (2001) Central pattern generators. In: Encyclopedia of Life Sciences, electronic press at www.ELS.net. Macmillan Reference
Ijspeert AJ (2008) 2008 special issue: central pattern generators for locomotion control in animals and robots: A review. Neural Netw 21:642–653
Ijspeert AJ, Crespi A, Ryczko D, Cabelguen JM (2007) From swimming to walking with a salamander robot driven by a spinal cord model. Science 315:1416–1420
Ijspeert AJ, Kodjabachian J (1999) Evolution and development of a central pattern generator for the swimming of a lamprey. Artif Life 5:247–269
Kopell N, Ermentrout GB (1986) Symmetry and phaselocking in chains of weakly coupled oscillators. Commun Pure Appl Math 39:623–660
Kopell N, Ermentrout GB (1988) Coupled oscillators and the design of central pattern generators. Math Biosci 90:87–109
Kristan WB, Stent GS, Ort CA (1974) Neuronal control of swimming in the medicinal leech. i. dynamics of the swimming rhythm. J Comp Physiol 94:97–119
Kuramoto Y (1984) Cooperatiave dynamics of oscillator community. a study based on lattice of rings. Progress Theor Phys Suppl 79:223–240
Marder E, Calabrese RL (1996) Principles of rhythmic motor pattern generation. Physiol Rev 76:687–717
Mulloney B, Smarandache C (2010) Fifty years of CPGs: two neuroethological papers that shaped the course of neuroscience. Front Behav Neurosci 4:45
Mulloney B, Smarandache-Wellmann C (2012) Neurobiology of the crustacean swimmeret system. Progress Neurobiol 96:242–267
Proctor J, Kukillaya RP, Holmes P (2010) A phase-reduced neuro-mechanical model for insect locomotion: feed-forward stability and proprioceptive feedback. Philos Trans R Soc Lond A 368:5087–5104
Ren L, Ermentrout B (1998) Monotonicity of phaselocked solutions in chains and arrays of nearest-neighbor coupled oscillators. SIAM J Math Anal 29:208–234
Schwemmer MA, Lewis TJ (2012) Phase response curves in neuroscience. In: Schultheiss NW, Prinz AA, Butera RJ (eds) The theory of weakly coupled oscillators. Springer, New York
Sigvardt KA, Miller WL (1974) Analysis and modeling of the locomotor central pattern generator as a network of coupled oscillators. Ann N Y Acad Sci 860:250–265
Skinner FK, Kopell N, Marder E (1994) Mechanisms for oscillation and frequency control in reciprocally inhibitory model neural networks. J Comput Neurosci 1:69–87
Skinner FK, Kopell N, Mulloney B (1997) How does the crayfish swimmeret system work? insights from nearest neighbor coupled oscillator models. J Comput Neurosci 4:151–160
Skinner FK, Mulloney B (1998) Intersegmental coordination of limb movements during locomotion: Mathematical models predict circuits that drive swimmeret beating. J Neurosci 18:3831–3842
Smarandache C, Hall WM, Mulloney B (2009) Coordination of rhythmic motor activity by gradients of synaptic strength in a neural circuit that couples modular neural oscillators. J Neurosci 29:9351–9360
Smarandache-Wellmann C, Weller C, Mulloney B (2014) Mechanism of coordination in distributed neural circuits: decoding and integration of coordinating information. J Neurosci 34:793–803
Stein PSG (2007) Motor pattern deletions and modular organization of turtle spinal cord. Brain Res Rev 57:118–124
Taylor AL, Cottrell GW, Kristan WB (2002) Analysis of oscillations in a reciprocally inhibitory network with synaptic depression. Neural Comput 14:561–581

Toth TI, Grabowska M, Rosjat N, Hellekes K, Borgmann A, Daun-Gruhn S (2015) Investigating intersegmental connections between thoracic ganglia in the stick insect by means of experimental and simulated phase response curves. Biol Cybern 109:349–362

Várkonyi PL, Kiemel T, Hoffman K, Cohen AH, Holmes P (2008) On the derivation and tuning of phase oscillator models for lamprey central pattern generators. J Comput Neurosci 25:245–261

Wang XJ, Rinzel J (1992) Alternating and synchronous rhythms in reciprocally inhibitory model neurons. Neural Comput 4:84–97

Williams TL, Sigvardt KA, Kopell N, Ermentrout GB, Remler MP (1990) Forcing of coupled nonlinear oscillators: studies of intersegmental coordination in the lamprey locomotor central pattern generator. J Neurophysiol 64:862–871

Zhang C, Guy RD, Mulloney B, Zhang Q, Lewis TJ (2014) The neural mechanism of optimal limb coordination in crustacean swimming. Proceedings of the National Academy of Sciences USA 111(38), 13,840–13,845

Zhang C, Lewis TJ (2013) Phase response properties of half-center oscillators. J Comput Neurosci 35:55–74